

# Observation of strong nuclear suppression in exclusive $J/\psi$ photoproduction in Au+Au ultra-peripheral collisions at RHIC

STAR Collaboration  
(Dated: November 28, 2023)

We report a measurement of exclusive  $J/\psi$  photoproduction in Au+Au ultra-peripheral collisions at  $\sqrt{s_{NN}} = 200$  GeV using the STAR detector. For the first time, i) the rapidity correlation between  $J/\psi$  photoproduction and neutron emission from nuclear breakups has been experimentally measured; ii) nuclear suppression factors are measured for both the coherent and incoherent  $J/\psi$  production. At photon-nucleon center-of-mass energy of 25.0 GeV, the coherent and incoherent  $J/\psi$  cross sections of Au nuclei are found to be  $71 \pm 10\%$  and  $36 \pm 7\%$ , respectively, of that of free protons. The stronger suppression observed in the incoherent production provides a new experimental handle to study the initial-state parton density in heavy nuclei. Data are compared with theoretical models quantitatively.

Keywords: ultra-peripheral collision, vector meson production, nuclear parton modification

The fundamental structure of protons and neutrons, collectively known as nucleons, is at the core of understanding modern physics. They are directly connected to problems of color confinement, the microscopic structures of visible matter, and the origin of dynamical mass generation from nonperturbative Quantum Chromodynamics (QCD). These problems are even more complex in the nuclear environment. Quark and gluon distributions for bound nucleons inside nuclei could be drastically different from those of the free nucleon. Understanding the fundamental structures of both nucleons and nuclei in a consistent framework is one of the most pressing tasks in high energy nuclear physics.

In recent years, vector meson photoproduction in ultra-peripheral collisions (UPC) of heavy ions has provided an excellent experimental probe to study the structures of nucleons and nuclei [1]. Typically, these photon-induced interactions take place at a large impact parameter and only produce one particle, e.g., the  $J/\psi$  meson [2]. In this reaction, the target nucleus may stay intact (coherent) or break up (incoherent), largely depending on the momentum transfer of the interaction.

Specifically, coherent  $J/\psi$  photoproduction has been extensively investigated by heavy-ion collider experiments [3–12], where the resulting cross sections are found to be significantly suppressed with respect to those of a free proton [4, 5, 11–13]. Many models attempt to explain this phenomenon [14–19], but the underlying mechanism remains highly debated [1]. On the other hand, the nuclear suppression of incoherent vector meson production has never been explicitly measured. Comparing incoherent vector meson production on a heavy nucleus and on a free proton is equivalent to comparing the parton structure of bound and free nucleons. This is one of the most direct and unambiguous approaches for studying bound nucleons in heavy-ion collisions. In addition, the incoherent production is a direct measure of nucleon and parton density fluctuation based on the Good-Walker paradigm [20], which provides a dynamical picture of the structure of nuclei at high energy.

In this Letter, we report measurements in

Au+Au UPCs at  $\sqrt{s_{NN}} = 200$  GeV using the STAR detector at the Relativistic Heavy-Ion Collider (RHIC). Specifically, we measure: i) coherent and incoherent  $J/\psi$  photoproduction cross sections on Au nuclei, associated with different neutron emission patterns as detected in zero degree calorimeters (ZDCs); ii) rapidity correlation between the  $J/\psi$  photoproduction and forward neutron emissions in both coherent and incoherent production; iii) nuclear suppression factors with respect to free nucleons. The photon-nucleon center-of-mass energy,  $W_{\gamma^*N}$ , is approximately 25.0 GeV for both coherent and incoherent processes at midrapidity in Au+Au UPCs [21]. The nuclear suppression data are compared with theoretical models: the nuclear shadowing model with leading twist approximation (LTA) [22, 23] and the saturation model color glass condensate (CGC) [17, 24].

The Solenoidal Tracker at RHIC (STAR) detector [25] and its subsystems have been thoroughly described in previous STAR papers [26, 27]. Charged particle tracking, including transverse momentum reconstruction and charge sign determination, is provided by the Time Projection Chamber (TPC) [28] positioned in a 0.5 T solenoidal magnetic field. The TPC volume extends from 50 to 200 cm from the beam axis and covers pseudorapidities  $|\eta| < 1.0$  over the full azimuthal angle,  $0 < \phi < 2\pi$ . The TPC also provides ionization loss ( $dE/dx$ ) measurement of tracks used for particle identification. Surrounding the TPC is the Barrel Electromagnetic Calorimeter (BEMC) [29], which is a lead-scintillator sampling calorimeter. The BEMC is segmented into 4800 optically isolated towers covering the full azimuthal angle for pseudorapidities  $|\eta| < 1.0$ . Between the TPC and BEMC is the Time Of Flight (TOF) system. It is finely segmented in  $\eta$  and  $\phi$  and provides fast trigger signals for charged particles in the range  $|\eta| < 0.9$ . There are two Beam-Beam Counters (BBCs) [30], one on each side of the STAR main detector, covering a pseudorapidity range of  $3.4 < |\eta| < 5.0$ . There are also two ZDCs [25], 18 m along each beam direction covering  $|\eta| > 6.7$ , used to monitor the luminosity and to tag forward neutrons.

The UPC data were collected by the STAR experi-

ment during the 2016 Au+Au run, which corresponds to an integrated luminosity of  $13.5 \text{ nb}^{-1}$  yielding approximately  $2.4 \times 10^7$  UPC  $J/\psi$  triggered events. The  $J/\psi$  candidates are reconstructed via the electron decay channel,  $J/\psi \rightarrow e^+e^-$ . Based on this channel, the UPC  $J/\psi$  trigger is defined by a topological selection of back-to-back clusters in the BEMC, a TOF charged track multiplicity between 2 and 6 (inclusive), and no BBC signal in either beam direction.

In the offline analysis, the events are required to have a pair of tracks with a vertex that is reconstructed within 100 cm of the center of the STAR detector along the beam direction. Tracks are required to have at least 15 points (out of a maximum of 45) to ensure sufficient momentum resolution, contain no fewer than 11 points for the ionization energy loss determination to ensure good  $dE/dx$  resolution, and to be matched to a BEMC cluster for consistency with the trigger. Electron pair selection is performed based on the  $dE/dx$  of tracks, where the dominant contamination at  $p_T \sim 1.5 \text{ GeV}/c$  is from pions. The variable  $n_{\sigma,e}$  ( $n_{\sigma,\pi}$ ) is the difference between the measured  $dE/dx$  value compared to an electron ( $\pi$ ) hypothesis of the predicted  $dE/dx$  value. It is calculated in terms of the number of standard deviations from the predicted mean. The pair selection variable  $\chi_{ee}^2$  is defined as  $n_{\sigma,e1}^2 + n_{\sigma,e2}^2$  for tracks 1 and 2, and similarly for the  $\pi$  pair hypothesis. Tracks consistent with electron pairs were selected by requiring  $\chi_{ee}^2 < 10$  and those consistent with pion pairs were rejected by requiring  $\chi_{ee}^2 < \chi_{\pi\pi}^2$ . The selections were performed separately for opposite-sign ( $+-$ ) and like-sign ( $++,--$ ) pairs. The like-sign pairs were taken as a measure of combinatoric backgrounds and subtracted from the opposite-sign pairs for final distributions.

Like-sign subtracted distributions of invariant mass  $m_{ee}$  and pair  $p_T$  were produced. Template distributions of signal  $J/\psi$  and background  $e^+e^-$  from Quantum Electrodynamics (QED) photon-photon interactions and  $\psi(2S)$  production were also created. The templates used output from the STARlight [31] Monte Carlo program weighted by the H1 data [32], which were passed through the GEANT3-based [33] STAR detector simulation to model the detector response. To extract the  $J/\psi$  yield, simultaneous fits of the templates to both the  $m_{ee}$  and pair  $p_T$  distributions were performed. For the differential cross section measurements in rapidity intervals, the same procedure was applied, and the  $J/\psi$  yields were extracted for both coherent and incoherent production. See the detailed procedure in Ref. [34].

The results were further divided into different neutron emission patterns as measured by the ZDCs, where neutrons can be produced by either the QED process of mutual Coulomb excitation [2] or nuclear breakup from hard scattering processes. The patterns of neutron emission are categorized as: i)  $0n0n$  - neither ZDC has detected a neutron; ii)  $0nXn$  - one ZDC has detected at least one neutron and the other has no neutrons; iii)  $XnXn$  - both ZDCs have detected at least one neutron. Results sum-

ming over these three categories are denoted as the *all n* category. Overlaps of ZDC hits from other events in the same RHIC bunch crossing caused migrations between these categories. This effect was measured in a sample of zero-bias data in terms of ZDC requirement, and the migrations were corrected for. This correction was up to 8% for the coherent  $J/\psi$  photoproduction cross section.

The differential cross section of  $J/\psi$  photoproduction as a function of  $p_T^2$  and rapidity  $y$  is measured in the Au+Au UPCs as follows,

$$\frac{d^2\sigma}{dp_T^2 dy_i} = \frac{N_{raw,i}}{\varepsilon_{trig} \cdot corr_i \cdot L \cdot BR \cdot \Delta p_{T_i}^2 \cdot 2\Delta y_i}. \quad (1)$$

Here  $\frac{d^2\sigma}{dp_T^2 dy_i}$  is the doubly differential cross section in  $(p_T^2, y)$  bin  $i$ , where  $i$  is a single index that includes all measured  $(p_T^2, y)$  combinations.  $N_{raw,i}$  is the raw number of  $J/\psi$  in bin  $i$ .  $\varepsilon_{trig}$  is an overall scale correction for trigger efficiency, and  $corr_i$  is the acceptance and efficiency correction for bin  $i$ . The integrated luminosity is denoted by  $L$ , and  $BR = 5.97\%$  is the branching ratio of  $J/\psi$  decaying into an electron and positron [35];  $\Delta p_{T_i}^2$  and  $\Delta y_i$  are the widths of bin  $i$ . The factor of 2 is introduced because  $J/\psi$  events are measured within  $|y| < 1$ , while the cross section is only reported for  $y > 0$ ; this factor is not included for the cross section  $d\sigma/dy$  for  $0nXn$  discussed later. The  $J/\psi$  acceptance corrections are based on the STARlight [31] MC events embedded into STAR zero-bias events, where a bin-by-bin unfolding technique is employed in the correction procedure as exhibited in Eq. 1.

For each rapidity of  $J/\psi$  there are two different contributions mixed together, a higher energy and a lower energy photon, which correspond to photons emitted by either nucleus. Based on the technique in Ref. [36], we resolve the photon energy ambiguity and measure the coherent  $J/\psi$  photoproduction cross section for  $\gamma + \text{Au} \rightarrow J/\psi + \text{Au}$ . The details of this procedure are outlined in the article Ref. [34] submitted along with this Letter.

Different sources of systematic uncertainty on the differential cross section were investigated, which are similar to the previous STAR publication on  $J/\psi$  photoproduction in deuterons [37]. The background subtraction using fit templates introduces uncertainties from the fitting, resulting in 10-20% on the background-subtracted distributions, depending on the  $J/\psi$  transverse momentum. Several factors contribute to the acceptance and efficiency corrections for pair mass and  $p_T$  distributions. The trigger efficiency determination results in final uncertainties  $\sim 8\%$ . The efficiency of matching tracks to BEMC energy deposits as measured with data has an uncertainty of  $\sim 5\%$  on the pair efficiency. The uncertainty on weighting of STARlight to match the  $p_T$  distributions is only significant on the steeply falling coherent  $J/\psi$  peak, where the pair detection efficiency uncertainty is up to 15%. The uncertainty from modeling radiative events in the simulation is  $\sim 2\%$  on pair acceptance. The background subtrac-

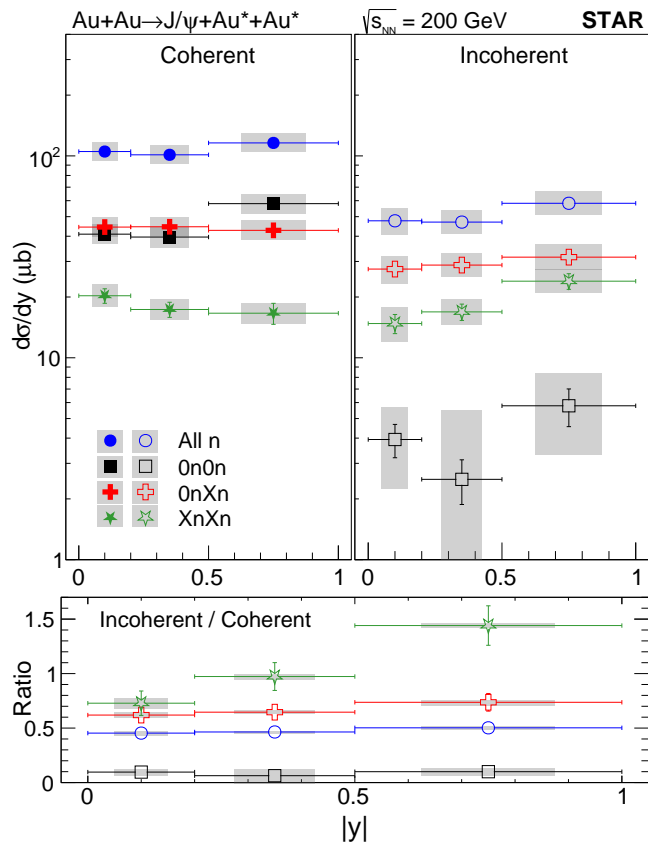


FIG. 1. Differential cross sections  $d\sigma/dy$  for coherent (top left) and incoherent (top right)  $J/\psi$  photoproduction and their ratios (bottom) as a function of  $|y|$  in Au+Au UPCs at  $\sqrt{s_{NN}} = 200$  GeV, for the different neutron categories defined in the text. Statistical uncertainties are represented by the error bars, and the systematic uncertainties are denoted as boxes. There is a systematic uncertainty on the cross sections of 10% from the integrated luminosity that is not shown.

tion and acceptance uncertainties were determined bin-by-bin in mass and  $p_T$  of electron pairs. They were added in quadrature along with an overall 4% uncertainty on track and vertex reconstruction efficiency; this sum is shown with the displayed data points. The systematic uncertainty on modeling the transversely polarized photon flux is found to be up to 3.5% by varying the Au radius  $\pm 0.5$  fm, where the same method has been adopted as in Ref. [37]. Finally, there is an uncertainty of 10% on the luminosity measurement, resulting in a scale uncertainty of 10% on all cross sections, which is not displayed in the figures.

In Fig. 1, the differential cross sections  $d\sigma/dy$  of  $J/\psi$  photoproduction as a function of  $|y|$  for coherent (left) and incoherent (right) production are presented, for *all n* data and each neutron category separately. They are obtained by integrating the data over low (coherent) or high (incoherent)  $p_T^2$  and using the template fits to correct to the full  $p_T^2$  range [34]. The rapidity interval includes both positive and negative rapidities, where the

data are plotted at the bin center. The ratio between incoherent and coherent  $J/\psi$  production is also shown in the bottom panel.

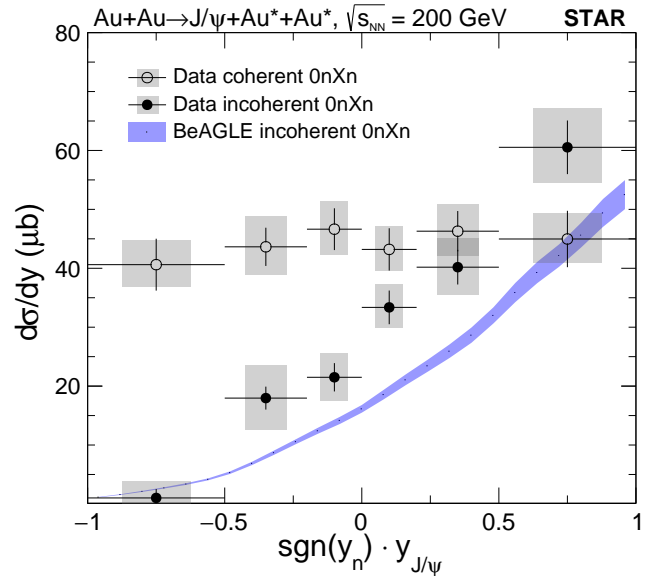


FIG. 2. Coherent and incoherent differential cross sections,  $d\sigma/dy$ , as a function of  $y$  of  $J/\psi$  photoproduction for the  $0nXn$  neutron configuration in Au+Au UPCs at  $\sqrt{s_{NN}} = 200$  GeV. Here the negative  $y$  direction has zero neutrons ( $0n$ ) and the positive  $y$  direction has at least one neutron ( $Xn$ ). Statistical uncertainties are represented by the error bars, and the systematic uncertainties are denoted as boxes. There is a systematic uncertainty of 10% from the integrated luminosity that is not shown. The BeAGLE model [38] is also shown.

To further investigate the rapidity dependence, the rapidity distributions for coherent and incoherent  $J/\psi$  photoproduction are shown for the asymmetric  $0nXn$  neutron category in Fig. 2. Positive  $J/\psi$  rapidity ( $\text{sgn}(y_n) \cdot y_{J/\psi}$ ) is defined by the direction of forward going neutrons,  $\text{sgn}(y_n)$ , where  $y_n$  is the neutron rapidity. The coherent  $J/\psi$  rapidity distribution is found to be symmetric under the transformation  $y \rightarrow -y$ . Neutron emission for coherent  $J/\psi$  photoproduction occurs through mutual Coulomb excitation, in which the neutron may be emitted by either nucleus. Thus, the neutron direction is not expected to be correlated to the  $J/\psi$  direction. Before this measurement, the assumption that neutron emission is independent of coherent vector meson photoproduction has never been experimentally tested. By contrast, in the incoherent process the target nucleus breaks up in the hard interaction, and neutrons hitting a ZDC identify the direction of the target nucleus; for the  $0nXn$  configuration, this direction is unambiguous. This result is also compared with an incoherent  $J/\psi$  production model, BeAGLE [38], which is found to be qualitatively consistent with the data.

In Fig. 3, the nuclear suppression factors of coherent

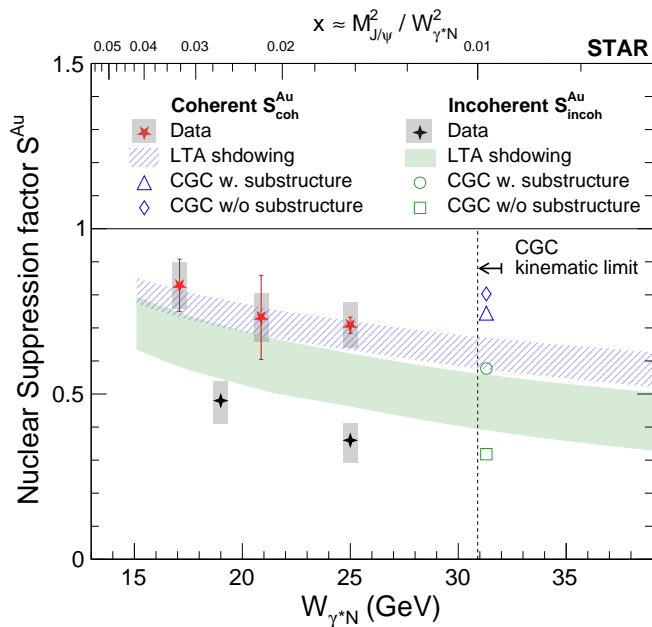


FIG. 3. Nuclear suppression factor of coherent ( $S_{\text{coh}}^{\text{Au}}$ ) and incoherent ( $S_{\text{incoh}}^{\text{Au}}$ )  $J/\psi$  photoproduction in Au+Au UPCs. The data are compared with the nuclear shadowing model [22] and the CGC model [17]. The CGC points are shifted from the vertical line for better visibility. Statistical uncertainties are represented by the error bars, and the systematic uncertainties are denoted as boxes. There is a systematic uncertainty of 10% from the integrated luminosity that is not shown.

( $S_{\text{coh}}^{\text{Au}}$ ) and incoherent ( $S_{\text{incoh}}^{\text{Au}}$ )  $J/\psi$  photoproduction are shown as a function of  $W_{\gamma^*N}$  in Au+Au UPCs. For the coherent case, the  $S_{\text{coh}}^{\text{Au}}$  is calculated based on the ratio between the coherent  $J/\psi$  cross section of *all*  $n$  and the Impulse Approximation (IA) [23], where IA represents the scenario without any nuclear effect. The suppression factor at  $W_{\gamma^*N} = 25.0$  GeV is found to be  $0.71 \pm 0.04 \pm 0.07 \pm 0.07$ . The first quoted error is the model uncertainty on IA [23] for Au nuclei and the second error is a combination of statistics and systematic uncertainties added in quadrature, while the third is from the scale uncertainty of the integrated luminosity.

For the incoherent suppression factor,  $S_{\text{incoh}}^{\text{Au}}$ , it is defined as the ratio between the incoherent  $J/\psi$  cross section of *all*  $n$  and the free proton data at HERA. In order to compare with photoproduction in  $ep$  collisions, we use the published H1 data and its well-constrained parametrization [32]. It is found that the STAR UPC incoherent  $p_T^2$  distribution is well described by the H1  $ep$  template, with a suppression factor found to be  $0.36_{-0.04}^{+0.03} \pm 0.04 \pm 0.04$  at  $W_{\gamma^*N} = 25.0$  GeV. Here the first uncertainty is the H1 parametrization uncertainty, the second one is from the measurement that includes statistical and systematic uncertainty, and the third is the scale uncertainty on the integrated luminosity. The details of this procedure, both for coherent and incoherent processes, are outlined in the article Ref. [34] submitted

along with this Letter.

The nuclear shadowing model LTA and the saturation model CGC are compared with the data quantitatively. For the LTA, the upper bound of each band is showing the weak shadowing mode, while the lower bound shows the strong shadowing mode [22]. It is found that, for the first time, the incoherent suppression factor is less than that of the coherent production, as well as the strong shadowing mode in the LTA model. For the CGC model, although it is not strictly calculated at the STAR kinematic range due to the applicability of the model ( $x > 0.01$ , where  $x$  is the momentum fraction the parton carries of the nucleon), the incoherent data are found to be between the model scenarios calculated with or without sub-nucleonic fluctuation of the parton density [17]. Based on this data, it is hard to conclude if sub-nucleonic parton density fluctuation is present in the incoherent  $J/\psi$  photoproduction, contrary to the conclusion to a recent measurement by the ALICE Collaboration [39]. Note that the  $p_T^2$  distribution of the incoherent production are found to be consistent between STAR and ALICE. Nevertheless, the reported data provides new insights to the nuclear parton density at RHIC.

In conclusion, differential cross sections of  $J/\psi$  photoproduction in coherent and incoherent processes as a function of rapidity  $y$  in Au+Au UPCs at  $\sqrt{s_{\text{NN}}} = 200$  GeV have been reported. These cross sections are measured separately in different neutron emission categories, as detected by the zero degree calorimeters. It is observed that in the asymmetric neutron configuration the coherent  $J/\psi$  production is independent of the neutron emission direction, while the incoherent production has a strong dependence. This is consistent with expectations from Monte Carlo simulations, but confirmed experimentally for the first time. Furthermore, the relative coherent cross section to that of a free nucleon is found to be  $71 \pm 10\%$  ( $\sim 30\%$  suppressed). The incoherent  $J/\psi$  photoproduction has been compared to that of a free proton based on the H1 data, where a stronger suppression than that of the coherent production is observed with a relative cross section of  $36 \pm 7\%$  ( $\sim 60\%$  suppressed). This is stronger than predictions from the nuclear shadowing model, and does not directly support the CGC model with sub-nucleonic fluctuation. The parton density at the top RHIC energy lies in the transition region ( $x_{\text{parton}} \sim 0.01$ ) between large momentum quarks ( $x_{\text{parton}} > 0.1$ ) and low momentum gluons ( $x_{\text{parton}} < 0.001$ ), which is essential to the understanding of both gluon saturation and nuclear shadowing mechanisms. This measurement provides important constraints to the parton density and is an essential experimental baseline for such measurements at the upcoming Electron-Ion Collider.

We thank the RHIC Operations Group and RCF at BNL, the NERSC Center at LBNL, and the Open Science Grid consortium for providing resources and support. This work was supported in part by the Office of Nuclear Physics within the U.S. DOE Office of Science, the

U.S. National Science Foundation, National Natural Science Foundation of China, Chinese Academy of Science, the Ministry of Science and Technology of China and the Chinese Ministry of Education, the Higher Education Sprout Project by Ministry of Education at NCKU, the National Research Foundation of Korea, Czech Science Foundation and Ministry of Education, Youth and Sports of the Czech Republic, Hungarian National Research, Development and Innovation Office, New National Excellency Programme of the Hungarian Ministry of Human

Capacities, Department of Atomic Energy and Department of Science and Technology of the Government of India, the National Science Centre and WUT ID-UB of Poland, the Ministry of Science, Education and Sports of the Republic of Croatia, German Bundesministerium für Bildung, Wissenschaft, Forschung und Technologie (BMBF), Helmholtz Association, Ministry of Education, Culture, Sports, Science, and Technology (MEXT), Japan Society for the Promotion of Science (JSPS) and Agencia Nacional de Investigación y Desarrollo (ANID) of Chile.

- 
- [1] M. Arslanok *et al.*, Hot QCD White Paper, (2023), [arXiv:2303.17254 \[nucl-ex\]](#).
- [2] C. A. Bertulani, S. R. Klein, and J. Nystrand, Physics of ultra-peripheral nuclear collisions, *Ann. Rev. Nucl. Part. Sci.* **55**, 271 (2005), [arXiv:nucl-ex/0502005](#).
- [3] S. Afanasiev *et al.* (PHENIX), Photoproduction of  $J/\psi$  and of high mass  $e+e-$  in ultra-peripheral Au+Au collisions at  $\sqrt{s_{NN}} = 200$ -GeV, *Phys. Lett. B* **679**, 321 (2009), [arXiv:0903.2041 \[nucl-ex\]](#).
- [4] V. Khachatryan *et al.* (CMS), Coherent  $J/\psi$  photoproduction in ultra-peripheral PbPb collisions at  $\sqrt{s_{NN}} = 2.76$  TeV with the CMS experiment, *Phys. Lett. B* **772**, 489 (2017), [arXiv:1605.06966 \[nucl-ex\]](#).
- [5] B. Abelev *et al.* (ALICE), Coherent  $J/\psi$  photoproduction in ultra-peripheral Pb-Pb collisions at  $\sqrt{s_{NN}} = 2.76$  TeV, *Phys. Lett. B* **718**, 1273 (2013), [arXiv:1209.3715 \[nucl-ex\]](#).
- [6] S. Acharya *et al.* (ALICE), Coherent photoproduction of  $\rho^0$  vector mesons in ultra-peripheral Pb-Pb collisions at  $\sqrt{s_{NN}} = 5.02$  TeV, *JHEP* **06**, 035 (2020), [arXiv:2002.10897 \[nucl-ex\]](#).
- [7] S. Acharya *et al.* (ALICE), First measurement of coherent  $\rho^0$  photoproduction in ultra-peripheral Xe-Xe collisions at  $\sqrt{s_{NN}} = 5.44$  TeV, *Phys. Lett. B* **820**, 136481 (2021), [arXiv:2101.02581 \[nucl-ex\]](#).
- [8] S. Acharya *et al.* (ALICE), First measurement of the  $|t|$ -dependence of coherent  $J/\psi$  photonuclear production, *Phys. Lett. B* **817**, 136280 (2021), [arXiv:2101.04623 \[nucl-ex\]](#).
- [9] S. Acharya *et al.* (ALICE), Coherent  $J/\psi$  and  $\psi'$  photoproduction at midrapidity in ultra-peripheral Pb-Pb collisions at  $\sqrt{s_{NN}} = 5.02$  TeV, *Eur. Phys. J. C* **81**, 712 (2021), [arXiv:2101.04577 \[nucl-ex\]](#).
- [10] R. Aaij *et al.* (LHCb),  $J/\psi$  photoproduction in Pb-Pb peripheral collisions at  $\sqrt{s_{NN}} = 5$  TeV, *Phys. Rev. C* **105**, L032201 (2022), [arXiv:2108.02681 \[hep-ex\]](#).
- [11] A. Tumasyan *et al.* (CMS), Probing small Bjorken- $x$  nuclear gluonic structure via coherent  $J/\psi$  photoproduction in ultraperipheral PbPb collisions at  $\sqrt{s_{NN}} = 5.02$  TeV, (2023), [arXiv:2303.16984 \[nucl-ex\]](#).
- [12] S. Acharya *et al.* (ALICE), Energy dependence of coherent photonuclear production of  $J/\psi$  mesons in ultra-peripheral Pb-Pb collisions at  $\sqrt{s_{NN}} = 5.02$  TeV, *JHEP* (2023) **10**, 119 (2023), [arXiv:2305.19060 \[nucl-ex\]](#).
- [13] B. Abelev *et al.* (ALICE), Coherent  $J/\psi$  photoproduction in ultra-peripheral Pb-Pb collisions at  $\sqrt{s_{NN}} = 2.76$  TeV, *Phys. Lett. B* **718**, 1273 (2013), [arXiv:1209.3715 \[nucl-ex\]](#).
- [14] M. Alvioli, L. Frankfurt, V. Guzey, M. Strikman, and M. Zhalov, Color fluctuation phenomena in  $\gamma A$  collisions at the LHC, *CERN Proc.* **1**, 151 (2018).
- [15] V. Guzey and M. Zhalov, Exclusive  $J/\psi$  production in ultraperipheral collisions at the LHC: constrains on the gluon distributions in the proton and nuclei, *JHEP* **10**, 207 (2013), [arXiv:1307.4526 \[hep-ph\]](#).
- [16] V. Guzey, M. Strikman, and M. Zhalov, Nucleon dissociation and incoherent  $J/\psi$  photoproduction on nuclei in ion ultraperipheral collisions at the Large Hadron Collider, *Phys. Rev. C* **99**, 015201 (2019), [arXiv:1808.00740 \[hep-ph\]](#).
- [17] H. Mäntysaari, F. Salazar, and B. Schenke, Nuclear geometry at high energy from exclusive vector meson production, (2022), [arXiv:2207.03712 \[hep-ph\]](#).
- [18] B. Sambasivam, T. Toll, and T. Ullrich, Investigating saturation effects in ultraperipheral collisions at the LHC with the color dipole model, *Phys. Lett. B* **803**, 135277 (2020), [arXiv:1910.02899 \[hep-ph\]](#).
- [19] T. Toll and T. Ullrich, Exclusive diffractive processes in electron-ion collisions, *Phys. Rev. C* **87**, 024913 (2013), [arXiv:1211.3048 \[hep-ph\]](#).
- [20] M. L. Good and W. D. Walker, Diffraction dissociation of beam particles, *Phys. Rev.* **120**, 1857 (1960).
- [21] Note that there is a  $-0.5$  GeV shift in the estimate of  $W_{\gamma^*N}$  at midrapidity  $|y| < 0.2$ , caused by the higher photon flux of the lower energy photon contribution; however, the effect of this shift is found to be negligible.
- [22] E. Kryshen, M. Strikman, and M. Zhalov, Photoproduction of  $J/\psi$  with neutron tagging in ultra-peripheral collisions of nuclei at RHIC and the LHC, (2023), [arXiv:2303.12052 \[hep-ph\]](#).
- [23] V. Guzey, E. Kryshen, M. Strikman, and M. Zhalov, Evidence for nuclear gluon shadowing from the ALICE measurements of PbPb ultraperipheral exclusive  $J/\psi$  production, *Phys. Lett. B* **726**, 290 (2013), [arXiv:1305.1724 \[hep-ph\]](#).
- [24] H. Mäntysaari and B. Schenke, Evidence of strong proton shape fluctuations from incoherent diffraction, *Phys. Rev. Lett.* **117**, 052301 (2016), [arXiv:1603.04349 \[hep-ph\]](#).
- [25] K. H. Ackermann *et al.* (STAR), STAR detector overview, *Nucl. Instrum. Meth. A* **499**, 624 (2003).
- [26] J. Adam *et al.* (STAR), Low- $p_T$   $e^+e^-$  pair production in Au+Au collisions at  $\sqrt{s_{NN}} = 200$  GeV and U+U collisions at  $\sqrt{s_{NN}} = 193$  GeV at STAR, *Phys. Rev. Lett.*

- 121**, 132301 (2018), [arXiv:1806.02295](https://arxiv.org/abs/1806.02295) [hep-ex].
- [27] J. Adam *et al.* (STAR), Measurements of  $W$  and  $Z/\gamma^*$  cross sections and their ratios in p+p collisions at RHIC, *Phys. Rev. D* **103**, 012001 (2021), [arXiv:2011.04708](https://arxiv.org/abs/2011.04708) [nucl-ex].
- [28] M. Anderson *et al.*, The Star time projection chamber: A Unique tool for studying high multiplicity events at RHIC, *Nucl. Instrum. Meth. A* **499**, 659 (2003), [arXiv:nucl-ex/0301015](https://arxiv.org/abs/nucl-ex/0301015).
- [29] M. Beddo *et al.* (STAR), The STAR barrel electromagnetic calorimeter, *Nucl. Instrum. Meth. A* **499**, 725 (2003).
- [30] C. A. Whitten (STAR), The beam-beam counter: A local polarimeter at STAR, *AIP Conf. Proc.* **980**, 390 (2008).
- [31] S. R. Klein, J. Nystrand, J. Seger, Y. Gorbunov, and J. Butterworth, STARlight: A Monte Carlo simulation program for ultra-peripheral collisions of relativistic ions, *Comput. Phys. Commun.* **212**, 258 (2017), [arXiv:1607.03838](https://arxiv.org/abs/1607.03838) [hep-ph].
- [32] C. Alexa *et al.* (H1), Elastic and Proton-Dissociative Photoproduction of  $J/\psi$  Mesons at HERA, *Eur. Phys. J. C* **73**, 2466 (2013), [arXiv:1304.5162](https://arxiv.org/abs/1304.5162) [hep-ex].
- [33] R. Brun, F. Bruyant, M. Maire, A. C. McPherson, and P. Zancarini, GEANT3, CERN-DD-EE-84-01, <https://cds.cern.ch/record/1119728> (1987).
- [34] Exclusive  $J/\psi$ ,  $\psi(2s)$ , and  $e^+e^-$  pair production in Au+Au ultra-peripheral collisions at RHIC, (2023), [arXiv:2311.13632](https://arxiv.org/abs/2311.13632) [nucl-ex].
- [35] P. A. Zyla *et al.* (Particle Data Group), Review of Particle Physics, *PTEP* **2020**, 083C01 (2020).
- [36] V. Guzey, M. Strikman, and M. Zhalov, Disentangling coherent and incoherent quasielastic  $J/\psi$  photoproduction on nuclei by neutron tagging in ultraperipheral ion collisions at the LHC, *Eur. Phys. J. C* **74**, 2942 (2014), [arXiv:1312.6486](https://arxiv.org/abs/1312.6486) [hep-ph].
- [37] M. Abdallah *et al.* (STAR), Probing the Gluonic Structure of the Deuteron with  $J/\psi$  Photoproduction in d+Au Ultraperipheral Collisions, *Phys. Rev. Lett.* **128**, 122303 (2022), [arXiv:2109.07625](https://arxiv.org/abs/2109.07625) [nucl-ex].
- [38] W. Chang, E.-C. Aschenauer, M. D. Baker, A. Jentsch, J.-H. Lee, Z. Tu, Z. Yin, and L. Zheng, Benchmark eA generator for leptonproduction in high-energy lepton-nucleus collisions, *Phys. Rev. D* **106**, 012007 (2022), [arXiv:2204.11998](https://arxiv.org/abs/2204.11998) [physics.comp-ph].
- [39] S. Acharya *et al.* (ALICE), First measurement of the  $|t|$ -dependence of incoherent  $J/\psi$  photonuclear production, (2023), [arXiv:2305.06169](https://arxiv.org/abs/2305.06169) [nucl-ex].